Atomically thin MXene/WSe2 Schottky heterojunction towards enhanced photogenerated charge carrier

Nag Riya, Saha Raima, Layek Rama Kanta, Bera Abhijit

DOI: 10.1088/1361-648X/ad172e

Atomically thin MXene/WSe_2 Schottky heterojunction towards enhanced photogenerated charge carrier

Riya Nag[a], Raima Saha[a], Rama Kanta Layek[b], and Abhijit Bera[a]*

[a]Department of Physics, Midnapore College (Autonomous), Raja Bazar Main Rd, 721101 Midnapore, India

[b]School of Engineering Science, Department of Separation Science, LUT University, FI-15210 Lahti, Finland

Email: abhijit.bera@midnaporecollege.ac.in

Abstract

Two-dimensional materials garner increasing interest in next-generation electronics and optoelectronic devices due to their atomic-thin nature and distinctive physical properties. Building on these advances, we present the successful synthesis of a heterostructure composed of the semi-metallic Ti_3C_2-MXene and the semiconducting WSe_2, in which the atomic layers are vertically aligned. The wet impregnation method effectively synthesizes an atomically thin Ti_3C_2-MXene/WSe_2 heterostructure characterized by AFM, Raman and TRPL analysis. In addition, the current-voltage characteristics at the heterostructure reveal the Schottky junction probed by the scanning tunneling microscopy and the conductive atomic force microscopy tip. The Schottky heterojunction also exhibits enhanced photocatalytic properties by improving the photogenerated charge carriers and inhibiting recombination. This work demonstrates the unique 2D-2D Ti_3C_2-MXene/WSe_2 vertical heterojunction possesses superior photon trapping ability and can efficiently transport photogenerated charge carriers to the reaction sites to enhance photocatalysis performance.

Keywords: Ti_3C_2 MXene, WSe_2 nanosheet, vertical heterojunction, charge transportation, photocatalyst.

1. Introduction

The current collection of 2D materials has increased to over several dozen so far. These include layered oxides, semiconducting and transition metal dichalcogenides (TMDs), insulating hexagonal boron nitride (h-BN), MXene, mono elemental atomic layers like silicene,

phosphorene, graphene, etc.[1, 2] Two-dimensional (2D) layered materials are a special group of materials in which van der Waals (vdW) interactions can stack the two-dimensional covalently linked atomic layers.[3-6] Because of their surface properties, extreme thinness at the atomic level, and layered structure, it is possible to stack different or similar 2D material systems on top of each other to create quasi-2D vertical heterojunctions without any chemical bonds.[7, 8] In comparison to their multilayer arrangements, the physical and chemical properties of a single layer or bi-layer of two-dimensional materials differ significantly.[9, 10] The two-dimensional heterojunctions also pose enhanced charge transfer across the planar interface upon illumination, showing better photovoltaic and photocatalytic effect performances.[11] So, contemporary nanoelectronic devices, p-n junctions, photodetectors, photovoltaic cells, photocatalytic systems, and thermoelectric components heavily depend on both vertical and lateral heterojunctions.[12-14]

In the two-dimensional transition metal dichalcogenides (TMDs) family, WSe_2 is a fascinating semiconducting material with exceptional optoelectronic applications that must be modified by engineering other 2D materials.[15] It helps to create vertical heterostructures through weak van der Waals forces, avoiding the presence of dangling bonds that are known to impede carrier transport.[16] These engineering in van der Waals homo- or heterostructures formation involving TMDs are currently under consideration for various electronic and optoelectronic applications, including integrated circuits, transistor designs, light-emitting diodes, photovoltaic devices, and photodetectors.[17-20] Using a single cocatalyst for designing stable WSe_2-based heterostructure to simultaneously mediate reaction pathways of electrons and retard the hole-induced photo-corrosion without sacrificing surface active sites. By leveraging the disparity in their work functions, 2D semimetal or metal-like materials are expected to establish a Schottky junction with semiconductors, typically formed at the interface between the semiconductor and metal.[12, 21] Moreover, including Schottky junctions can simplify the architecture in the electronics as mentioned above and optoelectronic applications, eliminating the need for an additional layer for controlled charge transportation.[22]

Pristine Ti_3C_2 MXene is a perfect 2D semimetal to create a Schottky heterojunction with semiconductors.[23-26] A new family of two-dimensional (2D) materials created by removing the intermediate element from the MAX phases ($M_{n+1}AX_n$) have piqued the interest of researchers due to their outstanding electrical conductivity and rich surface properties.[27-29] The exceptional conductivity of semimetal MXenes makes it the perfect material for contacts and interconnections. Surface termination groups play a significant role in the physicochemical characteristics of MXenes. Various fabrication techniques yield distinct surface termination

groups on MXenes. For instance, MXenes treated with HF predominantly feature -F terminations, while those treated with LiF/HCl tend to exhibit more -O terminations.[30, 31] The unique surface chemistry, favorable location of the Fermi level, and strong electrical conductivity make MXene a highly effective cocatalyst for improving the separation and transfer of photogenerated charge carriers.[26, 32-36] This enhances the photovoltaic and photocatalytic capabilities of transition metal dichalcogenides (TMDs).[36-38]

This study utilized chemical exfoliation and chemical etching methods to prepare monolayer and multilayer sheets of WSe_2 and MXene, respectively. Finally, a wet impregnation method was used to prepare a 2D-2D vertical heterostructure composite. We characterized a 2D MXene (semimetal)-2D WSe_2 (semiconductor) nanosheet vertical heterojunction utilizing STS and CAFM. This study aims to improve the photocatalytic performance of WSe_2 and MXene in degrading pollutant dyes. This enhancement is achieved by mitigating the recombination of electron-hole pairs, expanding the responsiveness to visible light, and optimizing the utilization efficiency of visible light. The 2D-2D MXene-WSe_2 vertical heterojunction device could be used as an excellent optoelectronic application.

2. Experimental section:

2.1. Materials: We purchased analytical grade chemicals of titanium aluminium carbide powder (with a purity>99%) from Nanoshel. Additionally, we obtained tungsten selenide powder (with a purity>99.8%) from Alfa Aesar and lithium fluoride (300-mesh), N-methyl-2-pyrrolidone (NMP) from Sigma Aldrich. For our experiments, we utilized ethanol from Merck and deionized (DI) water acquired from MilliQ Millipore ultrapure water filtration without requiring additional purification.

2.2. Exfoliation of WSe_2 nanosheets: The liquid exfoliation technique has been employed to prepare 2D WSe_2 nanosheets (both single and multilayer). Initially, a glass beaker dispersed 100 mg of WSe_2 in 10 mL of NMP. The dispersed solution was sonicated for 10 h in an ultrasonic bath while maintaining the bath temperature below 8°C to reduce heat generation during exfoliation. After completing the sonication process, the well-dispersed solution was left undisturbed to settle for one day. The well-dispersed portion of the solution was descended and centrifuged at 1500 rpm for 45 min to collect the supernatant containing 2D WSe_2 nanosheets. Ethanol was added to the decanted part, followed by several rounds of centrifugation at 3000 rpm for 15 min each to collect the precipitate. NMP was replaced by adding ethanol to this collected well-dispersed NMP solution. The precipitate containing WSe_2 nanosheets (single and multilayer) was collected through several rounds of centrifugation.

2.3. Synthesis of Ti_3C_2-MXene nanosheets: The process of delaminating Ti_3C_2-MXene nanosheets from the MAX phase powder (Ti_3AlC_2) involves the removal of aluminium (Al) layers through an HCl+LiF chemical etching process. 0.3 g of LiF powder was added to 6 mL of 6 M HCl in a Teflon-coated beaker to create a proper HCl+LiF etching solution under magnetic agitation. 0.3 g MAX phase powder was added slowly and continuously in an ice bath to reduce the heat produced during the chemical reaction. Black MXene clay was formed by constantly stirring the mixture for 24 hours at room temperature. After that, distilled water was added to the black suspension and washed several times to reach a neutral pH value of the supernatant solution. The black clay-like sediment was then collected in a petri dish containing monolayer and multilayer MXene nanosheets. The sample was dried at 60 °C and stored in a vacuum-sealed refrigerator.

2.4. Synthesis of MXene-WSe_2 heterostructure: To prepare MXene-WSe_2 (2:8 wt%) heterostructure, we have prepared 1 mg/ml concentrate ethanolic solution of WSe_2 and MXene by sonication process. Two different solution was mixed in a beaker and magnetically stirred for 2 h at 60 °C in ambient. Once the process was completed, the well-dispersed solution was allowed to settle for 30 minutes. Then, the prepared sample was washed by centrifugation, and the collected sediment was dried with a vacuum drier.

2.6. Device fabrication: The current-voltage (I-V) characterization of the device uses a sandwich device configuration as (ITO|active layer|ITO). The etched substrate undergoes a continuous cleaning by successive immersion in soapy water, DI water, acetone, and alcohol for 15 min each, ensuring a thorough cleaning. To prepare a consistently thick layer of MXene-WSe2, a well-dispersed aqueous solution was drop-cast onto an etched ITO substrate. The film was dried in a desiccator for 30 min.

2.7. Photocatalytic activity Test: In a standard photocatalytic experiment of MB, a specified amount (0.5 mg/ml) of the photocatalyst is suspended in a 15 mL aqueous MB solution (10 mg/L) prepared using DI water. A 15 ml suspension of dye and photocatalyst was mechanically agitated for 30 minutes in an ultrasonic bath to achieve the proper adsorption-desorption equilibrium in the dark condition. This was followed by exposure to Xe lamp illumination for 1 hour for photodegradation. The progress of photodegradation was monitored by measuring the absorbance at 662 nm, which is the λ_{max} of MB, at 20-minute intervals.

The degradation efficiency was calculated using the following formula.

Degradation efficiency = $(1 - c/c_0) \times 100\%$

where the dye concentrations at t = 0 and t = t are denoted by the variables c0 and c, respectively. The kinetics of the photocatalytic reaction were evaluated using the first-order differential equation:

$\ln (c/c_0) = - kt$

$\ln (c_0/c) = kt$

Where k is the pseudo-first-order reaction velocity constant in min^{-1}.

2.8. Characterization:

The topographical investigation of 2D materials was performed by an XE-7, Park AFM. The images were obtained in non-contact mode AFM operation at a scan rate of 1.0 Hz in standard environmental conditions.

The CAFM measurements were performed using XE-7 Park AFM, which studied the morphological image and electrical signal channels like current, conductance, etc. The measurements were performed in ambient using commercial metal Pt/Ir coated etched Si tip and highly doped n-type Si substrate. The connection of the Si substrate was fixed using a silver paste. At first, we conducted imaging over broad surface areas without applying any bias to identify specific regions of interest on the sample surface. Subsequently, we scanned the same surface position in contact mode by applying a bias to get the current imaging.

The STM characterization was conducted using an XE-7 Park AFM in STM mode, operating under ambient conditions. All STM images were obtained in a constant-current mode with a scan rate of 0.5 Hz using Pt/Ir tip. To determine the location of conduction and valence band edges of the individual 2D materials, we measured the tunneling current (I) of ultrathin films by applying some bias voltage between the HOPG substrate and the conducting tip. The derivative of the tunneling current with respect to voltage (dI/dV) is directly proportional to density-of-state (DOS). The edges of dI/dV help pinpoint the semiconductor band edges (CB and VB) relative to the Fermi level at 0V. As a result, the bandgap of the materials under study can be detected from the difference between the CB and VB edge position and the location of the Fermi energy.

3. Result and discussion:

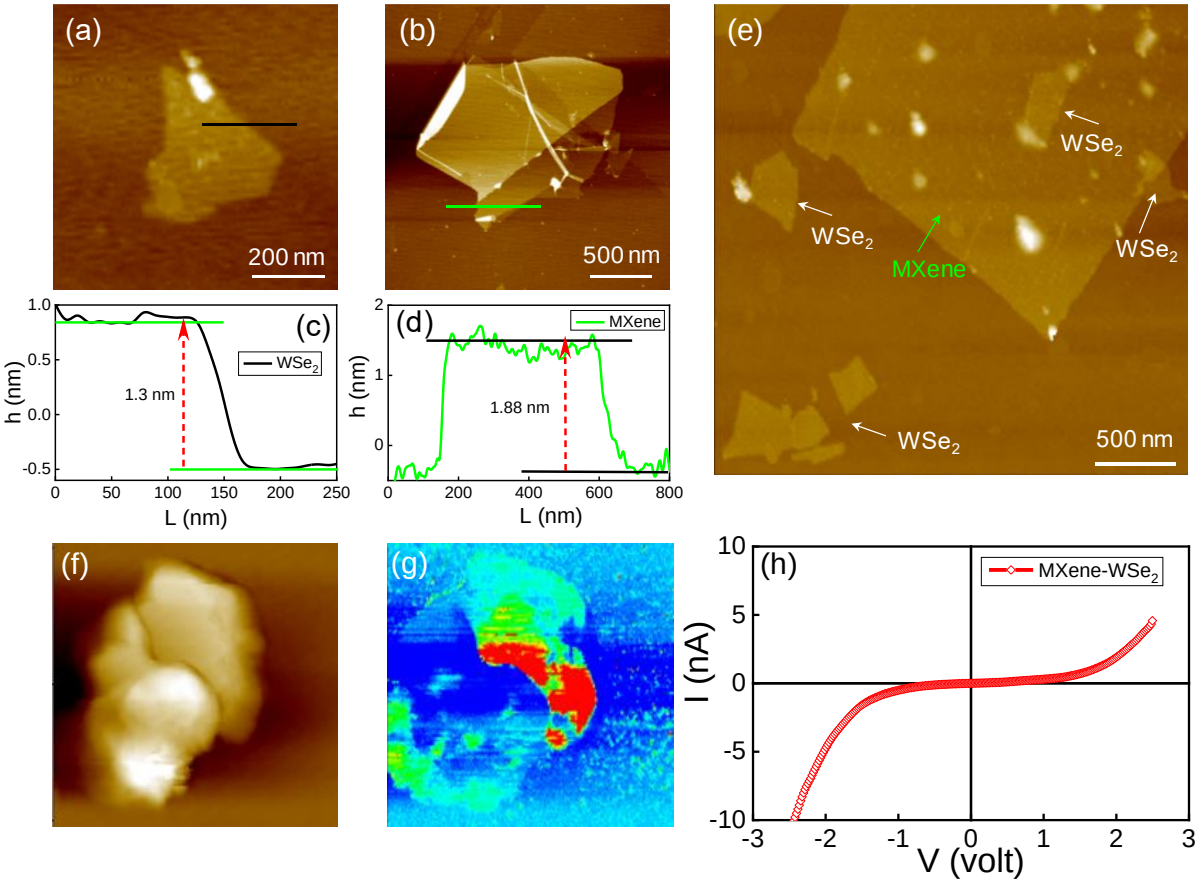

Figure 1: The morphological image by AFM of WSe_2 with corresponding line profile (a,c), MXene with corresponding line profile (b,d), MXene-WSe_2 heterostructure (e) and current-voltage characteristics by CAFM of MXene-WSe_2 heterostructure: topographical image (f) corresponding current image with bias voltage (g) and I-V characteristics (h).

The atomically thin nature of the synthesized 2D materials was first investigated by atomic force microscopy (AFM). Figures 1a, b and e represent the AFM topographical image of the pristine and vertical heterostructure of 2D materials. The images were scanned in non-contact mode AFM in ambient conditions. Figure 1a,b exhibits separate layers of a pristine WSe_2 nanosheet and Ti_3C_2 MXene, revealing an average lateral dimension of (350±50) nm and (2.0±0.5) μm, respectively. The line profiles of these nanosheets in Figures 1c and 1d reveal a thickness of (1.3±0.4) nm and (1.9±0.5) nm, indicating a few-layer nanosheet of WSe_2 and MXene, respectively.[39, 40] Figure 1e presents the formation of a vertically aligned heterostructure by WSe_2 nanosheet on the MXene surface.

Here, we aim to analyze the current-voltage (I-V) characteristics of the vertical MXene-WSe_2 heterostructure using conductive atomic force microscopy (CAFM). In CAFM, a platinum-

coated conductive tip scans the sample surface in contact mode. An electrical bias voltage between the tip and the sample is applied to record the I-V characteristics and current image as a function of lateral position. Figure 1f represents a CAFM topographical image of the stacked layer heterostructure, confirmed by the corresponding current image of the same heterostructure using a +6 V bias (Figure 1g). The I-V characteristics in Figure 1h on the vertical junction define rectifying nature presumable due to MXene-WSe_2 heterostructure. The vertical heterojunction is formed by 2D semiconducting WSe_2, and conducting MXene is the reason behind the observed disparity in the current image.

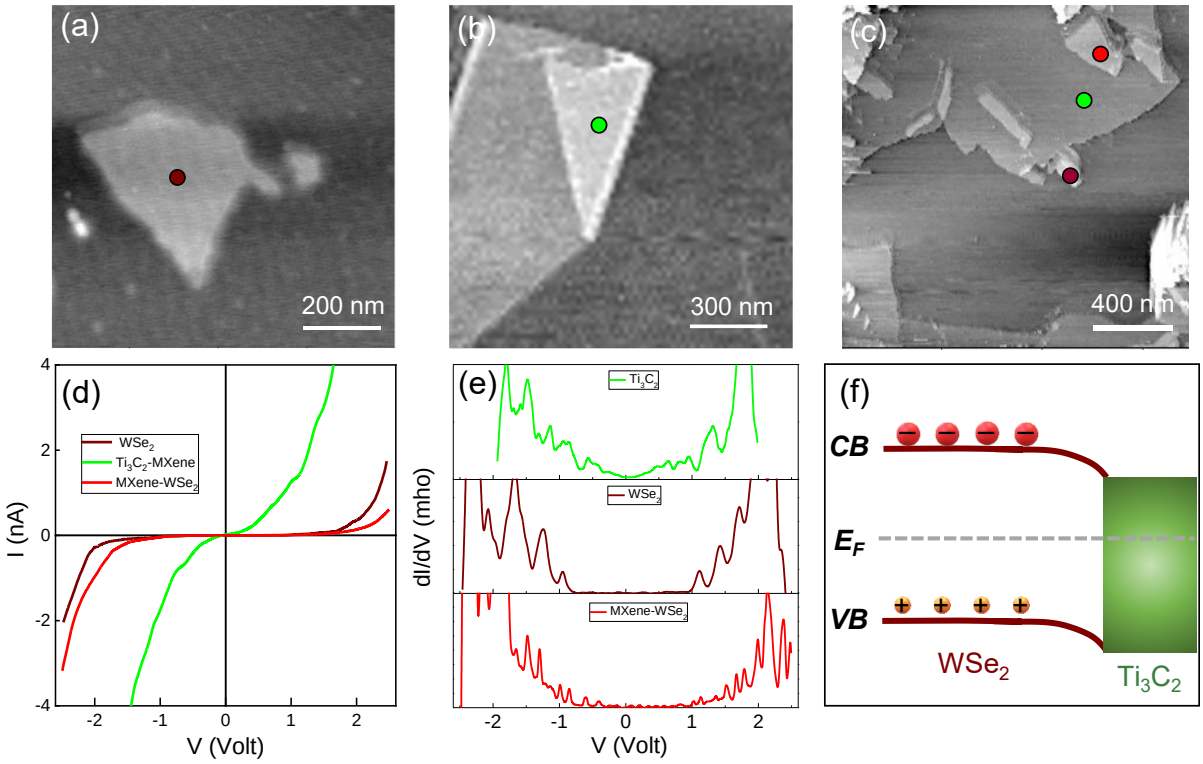

Figure 2. STM/S characterization of the vertical MXene-WSe_2 heterostructure: STM topographical image of pristine WSe_2 nanosheet (a) MXene nanosheet (b) and MXene-WSe_2 heterostructure (c). (d-e) I-V spectroscopy (d) and corresponding dI/dV spectra (e) of pristine and MXene-WSe_2 heterostructure at different positions of the layers as marked in colour circles. (f) Band diagram of MXene-WSe_2 vertical heterojunction.

To understand the band diagram of the heterostructure, we have studied the electronic characteristics of pristine and heterostructure 2D materials by utilizing scanning tunnelling microscopy (STM) along with scanning tunnelling spectroscopy (STS). For this purpose, an ultra-dilute nanosheet solution was drop cast on a highly oriented HOPG substrate and scanned using a Pt/Ir tip with a fixed scan rate. Figures 2a, b and c exhibit STM morphology of pristine

WSe_2 nanosheet, MXene nanosheet and MXene-WSe_2 heterostructure, respectively. Furthermore, to determine the location of conduction and valence band edges of the individual 2D materials, we measured the tunnelling current (I) of ultrathin films concerning applied bias voltage at different locations of the layer. As dI/dV spectra are directly proportional to density-of-state (DOS), the edges of dI/dV help pinpoint the conduction and valance band edge relative to the Fermi level at 0 V, revealing the electronic band gap of materials.[41] Figure 2d,e shows the I-V and corresponding dI/dV spectra of the WSe_2 nanosheet (wine), pristine MXene layer (green), and MXene-WSe_2 heterostructure (red). The I-V and dI/dV spectra of the MXene layer (green) support the metal-like behaviour, whereas the spectra of the WSe_2 nanosheet (green) indicate CB and VB band edges at +1.10 V and -0.85 V, respectively, revealing the semiconducting nature of WSe_2 nanosheets with an electronic band gap of (1.95±0.15) eV. Since the VB edge is closer to the Fermi level, aligned at 0 V, it implies a mild p-type semiconducting nature that could form a metal-semiconductor junction with MXene. The I-V characteristics of vertical MXene-WSe_2 heterojunction (Figure 2d, red) reveal a rectifying nature presumable due to the band bending at the interface. This can be explained by drawing a schematic band diagram of the MXene-WSe_2 interface, shown in Figure 2f. Additionally, some states close to the Fermi level arise in the dI/dV spectra of the MXene-WSe_2 system (Figure 2e, red), suggesting band hybridization, which experiences perturbation of electronic structure.[38] However, the rectifying behaviour and band diagram of the MXene-WSe_2 interface strongly suggest the formation of Schottky junctions.

The atomically thin Schottky heterojunction formed by MXene and WSe_2 could be exploited as a potential candidate for optoelectronic applications. For practical applications, a large amount of such heterostructure materials is needed. So, a wet impregnation method was employed to synthesize the atomically thin Ti_3C_2-MXene/WSe_2 heterostructure. XRD, Raman and XPS analysis further characterize the materials to confirm the successful synthesis.

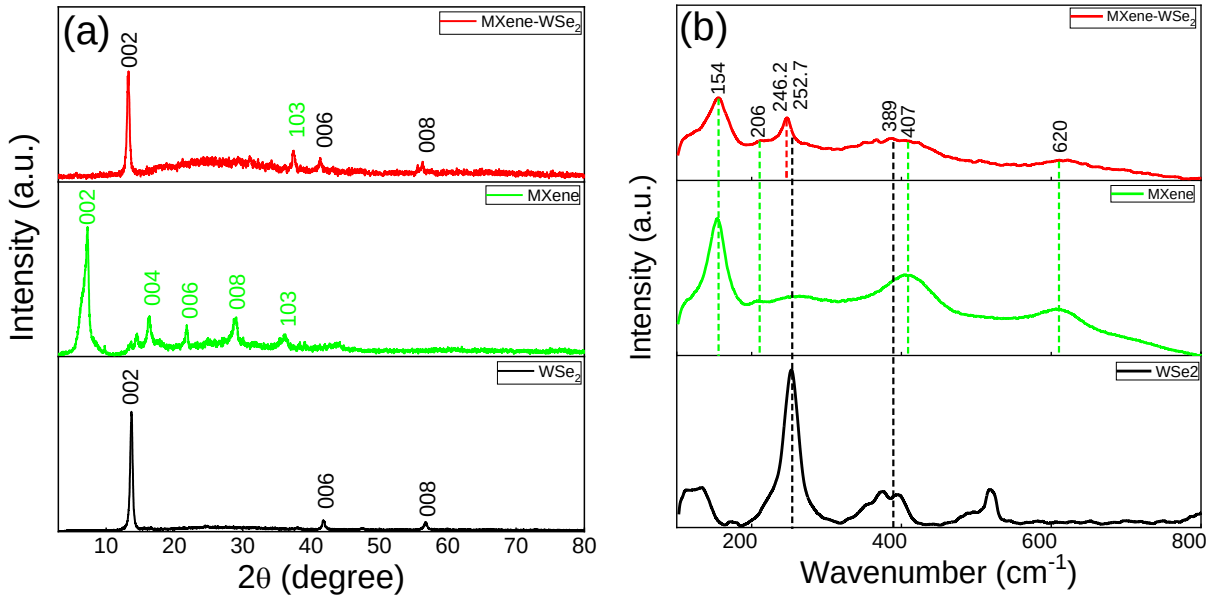

Figure 3: Structural property of MXene-WSe_2 heterostructure: (a) XRD pattern: (b) Raman spectroscopy of pristine WSe_2 (black), MXene (green) and MXene-WSe_2 (red).

The crystalline structure and phase compositions of exfoliated WSe_2, MXene, and MXene-WSe_2 composites were identified using X-ray diffraction (XRD) spectra, as shown in Figure 3a. Pristine WSe_2 nanosheets exhibit intense peaks at 13.7°, 41.7°, and 56.8°, in agreement with the (002), (006), and (008) diffraction planes of the hexagonal WSe_2. In contrast, the XRD pattern of pristine MXene shows the presence of (002), (004), (006), (008) and (103) diffraction planes at 7.2°, 16.2°, 21.7°, 28.8° and 36.16° respectively.[19, 26, 42] The X-ray diffraction (XRD) analysis of the MXene-WSe_2 hybrid reveals a combination of XRD lattice orientations from the MXene and WSe_2 phases. A blue shift (0.5°) of the major peak of WSe_2 in MXene-WSe_2 heterostructure may arise due to the increase of interlayer distance following the hybridization process.

The atomically thin nature of the composite and the heterostructure formation were further confirmed by Raman spectroscopy analysis. WSe_2 nanosheets exhibit a well-distinguished Raman peak at 252.7 $cm^{-1,}$ corresponding to the A1g mode without any shoulder peak, ensuring the proper exfoliation of WSe_2 from its bulk precursors.[19] The Raman spectra of MXene reveal distinct bands located at 154, 206, 407, and 620 cm^{-1}, which can be attributed to the vibration mode associated with Ti-C bonds. The broadness of existing peaks supports the good exfoliation of 2D MXene from its MAX phase precursors using the chemical etching method. The Raman mode of WSe_2 situated at 252.7 cm^{-1} exhibits a blue shift of 6 cm^{-1} upon the hybridization with MXene in the MXene-WSe_2 heterostructure.[10] This shift is attributed to the interaction characteristics, suggesting an interlayer coupling between WSe_2 and MXene at

the 2D/2D interface. This confirms the formation of atomically thin heterostructure by MXene and WSe_2 nanosheets.

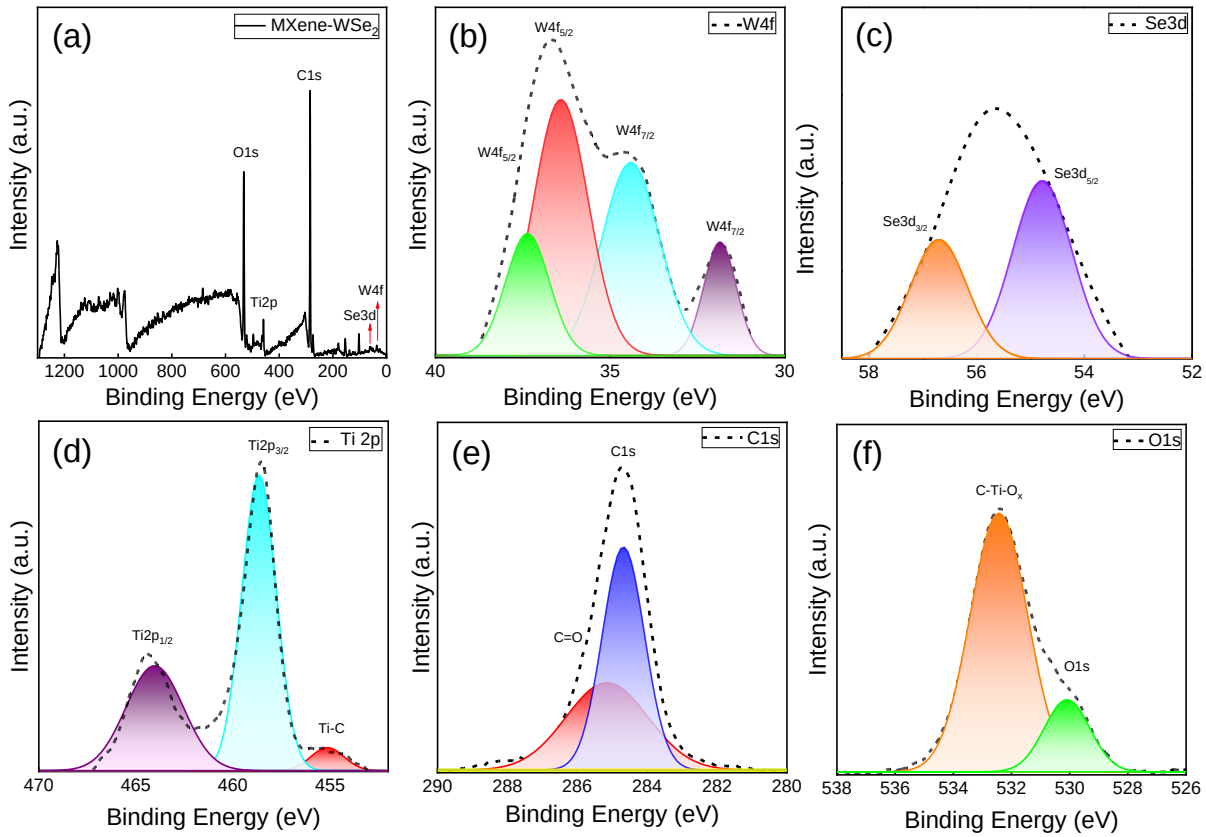

Figure 4: XPS spectra of MXene-WSe_2 hybrid: (a) Survey spectrum of MXene-WSe_2. (b-e) Core-level spectra of individual elements and deconvolution of distinct peaks.

X-ray photoelectron spectroscopy (XPS) determines the chemical compositions and oxidation state of MXene-WSe_2 heterostructure materials, as shown in Figure 4. The survey XPS spectra in Figure 4a reveal the presence of W, Se, Ti, C, and O based on their binding energies. The peaks corresponding to the $W4f_{5/2}$ and $W4f_{7/2}$ states are situated at 34.2 and 31.8 eV and along with 36.7 and 35.7 eV in Figure 4b, signifying the presence of the +4-oxidation state of W additionally with the +6-oxidation state of the surface W, respectively. As demonstrated in Figure 4c, the Se $3d_{3/2}$ and Se $3d_{5/2}$ peaks are located at 56.2 and 54.9 eV, respectively, suggesting that the Se within the heterostructure material maintains a stable oxidation state of -2. This observation agrees with a prior report on WSe_2.[9, 19] Figure 4d displays high-resolution XPS in the Ti 2p region, revealing two peaks corresponding to Ti $2p_{1/2}$ and Ti $2p_{3/2}$ at 463.8 and 458.5 eV binding energies. With the high sensitivity of XPS for identifying components at the core level of materials, a well-resolved Ti-C peak can be detected in the

heterostructure, suggesting the presence of MXene in the sample. Based on the deconvoluted XPS spectra of the C 1s peak in Figure 4e, we can detect different fractions of the bonding state of C-O and C–C at 285.2 and 285.2 and 284.6 eV binding energy, respectively. The analysis of the O 1s spectra in Figure 4f for the MXene-WSe_2 heterostructure reveals the presence of at least two distinct chemical bonding states on their surfaces, denoted as C-Ti-OH_x and O1s.[43]

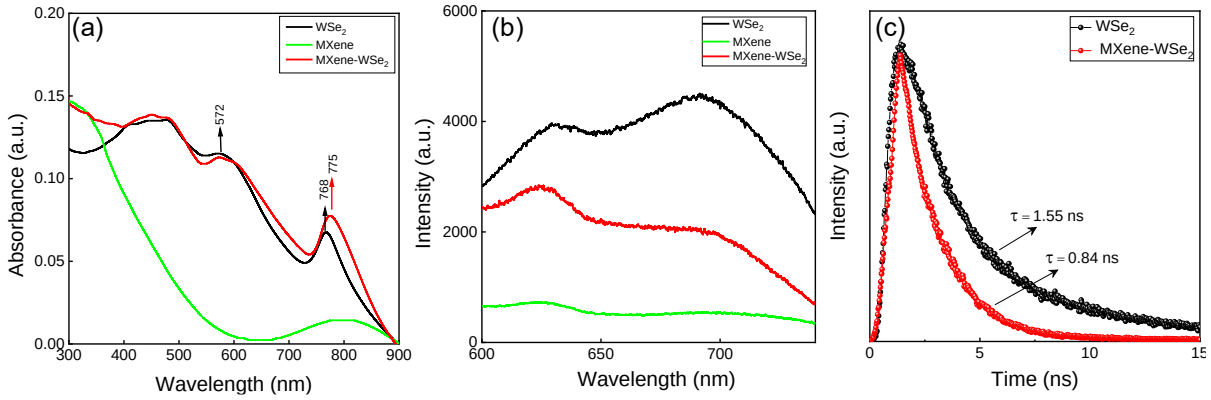

Figure 5: Optical characteristics: (a) UV-visible spectroscopy, (b) Photoluminescence spectra, and (c) TRPL spectra of pristine WSe_2 (black), MXene (green) and MXene-WSe_2 (red)

Analysis of optical absorption spectra aims to gain insight into the absorption properties of materials within the solar spectrum. Figure 5a reveals the UV-visible spectra of pristine WSe_2, MXene and MXene-WSe_2 heterostructure in their well-dispersed solution. It can be seen from the absorbance profile of pristine WSe_2 and MXene exhibits a broad range of light responsivity, which extends into the near-infrared (NIR) region. The absorption spectra of WSe_2 nanosheets indicate the presence of two distinct excitonic resonances occurring at wavelengths of 768 nm and 572 nm, respectively.[44] The optical absorbance of pristine MXene exhibits a strong peak at 320 nm and a relatively lower intense peak at 800 nm, supporting the proper exfoliation of MXene nanosheet from its bulk MAX phase precursors. The synthesized MXene exhibits a broad surface plasmon resonance (SPR) peak spanning from 620 to 900 nm, consistent with its metallic conductivity properties.[45] The absorbance spectrum of the MXene-WSe_2 heterostructure material presents a similar absorption spectrum compared to that of pristine WSe_2. The rise in absorbance intensity within the spectrum ranging from 300 to 400 nm, accompanied by a minor shift in the peak of excitonic resonances to 768 nm (redshift), is in good accordance with the formation of a heterostructure which suggests a change in the electronic or structural properties of the materials.

To investigate the recombination probability of light-induced electron and hole pairs, we studied photoluminescence spectroscopy of pristine WSe_2, MXene and MXene-WSe_2 heterostructure presented in Figure 5b with an excitation wavelength of 570 nm. The higher intensity of PL spectra of pristine WSe_2 indicates a greater recombination probability of photoexcited charge carriers. The PL intensity is lower for fabricated MXene-WSe_2 heterostructure, revealing comparatively lower charge recombination, hence greater charge transfer efficiency at the interface. Therefore, we investigated the time-resolved photoluminescence spectra of WSe_2 and MXene-WSe_2 heterostructure to explore the dynamics of charge transfer in the heterostructure. Figure 5c demonstrates that the MXene-WSe_2 heterostructure exhibits a significantly reduced fluorescence lifetime ($\tau = 0.84$ ns) compared to the pristine WSe_2 semiconductor ($\tau = 1.55$ ns). This decrease can be attributed to a more efficient nonradiative decay pathway in MXene-WSe_2 due to the electron transfer process from WSe_2 to MXene, consistent with PL analysis.[46] The enhancement of charge transfer efficiency at the interface may be created due to the incorporation of MXene in the heterostructure, as MXene acts as a potential material for charge trapping. The considerable potential of MXene as an electron and hole-trapping material can help create Schottky junctions to enhance the catalytic performance and durability of photosensitive semiconductors.

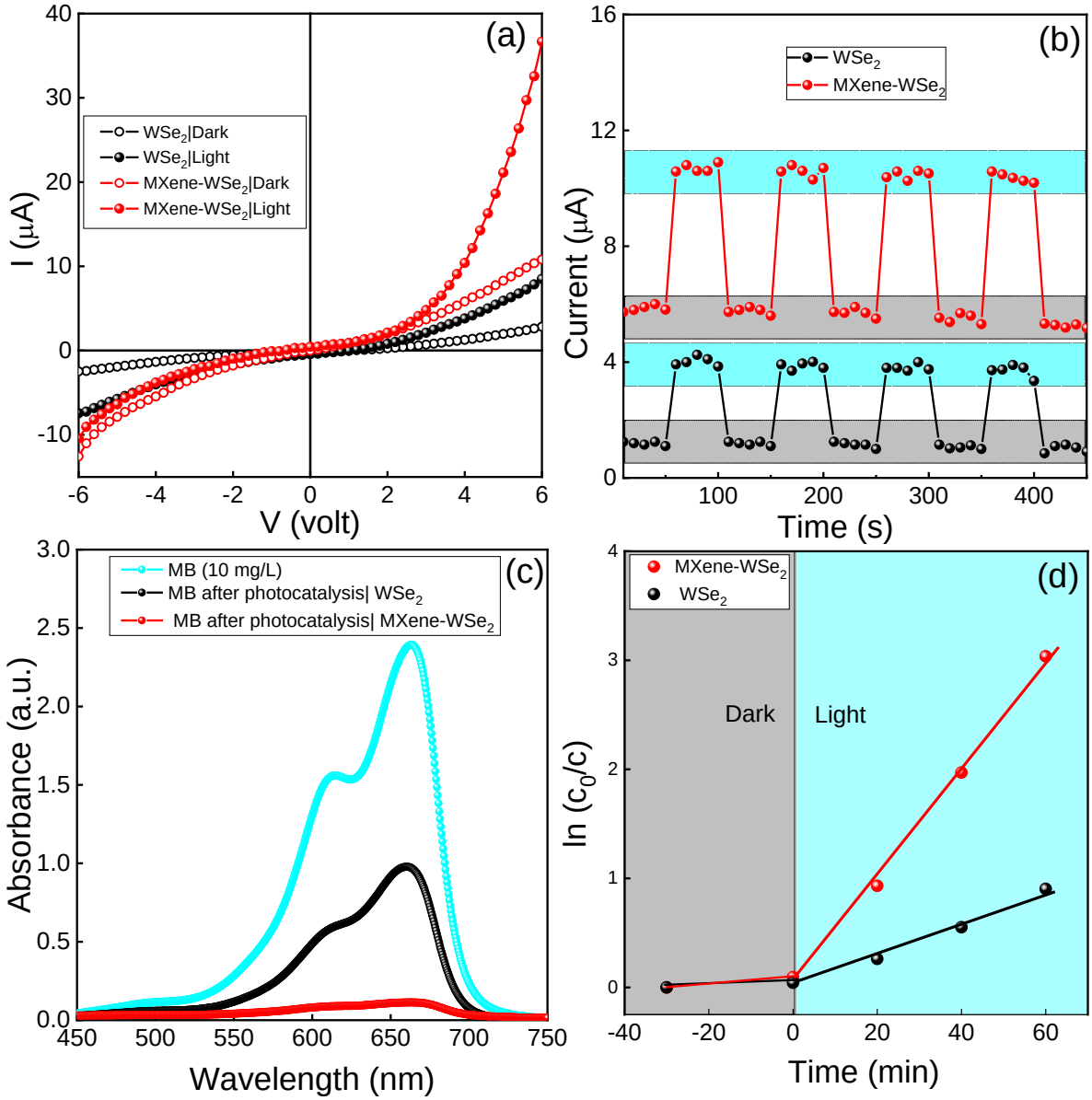

Figure 6: Photovoltaic and Photocatalytic response: (a) current−voltage (I−V) characteristics, (b) Photocurrent measurement of WSe_2 and MXene-WSe_2 heterostructure device on an ITO electrode under dark and Xenon light irradiation conditions. (c) Photocatalytic degradation profile and (d) photocatalytic reaction kinetic profile.

The charge transfer properties and the number of photogenerated charge carriers in both pristine WSe_2 devices and the MXene-WSe_2 heterostructure device were determined by analyzing their I-V characteristics. Figure 6a shows the current-voltage characteristic of fabricated devices with a simple device structure of (ITO | active layer | ITO) under dark and light conditions. The MXene-WSe_2 heterostructure device significantly improves current under illuminated conditions compared to the other devices. This enhancement of current under

illumination in one direction of heterostructure promotes efficient charge separation at the metal-semiconductor heterojunctions.

We measured the same devices under light exposure to evaluate the photogenerated charge carriers and stability of the device's performance. As shown in Figure 6b, there is a substantial increase in current for both pristine and heterostructure with light switching. For both WSe_2 and MXene-WSe_2 heterostructure, we have plotted the current magnitude at a +4 V bias before and after illumination as a function of time. The relatively enhanced photocurrent of the heterostructure device is primarily attributed to the vertical heterojunction formed at the metal-semiconductor interface between the conducting MXene and the semiconducting WSe_2 nanosheets. This interface promotes more efficient transportation of photogenerated charge carriers, reducing recombination losses and resulting in increased photocurrent. Hence, enhancing the conductive efficiency of photoactive charges and reducing the recombination probability of charge carriers supports the successful fabrication of 2D/2D MXene-WSe_2 vertical heterojunction at their interface, showing enhanced photocatalytic properties.

A selective photocatalytic degradation experiment of methylene blue (MB) in an aqueous solution was conducted under visible light exposure to determine whether the incorporation of highly conducting MXene into MXene-WSe_2 heterostructure can enhance the extraction of photogenerated electrons from WSe_2. A complete photocatalytic experiment was conducted under a 300W xenon lamp for the photocatalytic decomposition of methylene blue (MB) to compare the performance of pristine WSe_2 and MXene-WSe_2 heterostructures as a photocatalyst. The experiment also assessed the adsorption properties of WSe_2 and MXene-WSe_2 for methylene blue (MB) under identical experimental conditions. The simulated industrial wastewater of dye was continuously sonicated for 30 min to establish an adsorption-desorption equilibrium without light, which exhibited separate adsorption data for pristine and heterostructure samples. The superior adsorption performance of the MXene-WSe_2 catalyst can be attributed to the abundance of surface functional groups such as -OH, -F, and -O within MXene. Adsorption can enhance catalytic effects by capturing target pollutants on the catalyst, facilitating full contact between the active centres on the surface of the catalyst and the pollutants. This, in turn, results in an improvement in catalytic efficiency.

We evaluated the absorbance of methylene blue (MB) at a specific wavelength after 20 minutes of continuous light exposure for 1 hour to assess the degradation rate of dyes. The absorbance profile in Figure 6c shows that methylene blue undergoes nearly complete decomposition (95.2 %) within 1 hour when using the MXene-WSe_2 heterostructure photocatalyst. The degradation rates for WSe_2 and MXene-WSe_2 photocatalysts were calculated from $\ln(c_0/c)$

plots versus time, as depicted in Figure 6d. The velocity constant (k) was determined using the first-order differential equation of reaction kinetics and was found to be 0.014 min^{-1} and 0.045 min^{-1} for WSe_2 and MXene-WSe_2 heterojunction, respectively. The light illumination on MXene-WSe_2 Schottky heterojunction promotes rapid charge transfer, thus enhancing the photocatalytic degradation rate of MB. The easy transportation of charge in Schottky heterojunction upon illumination can generate an adequate number of active radicals participating in MB degradation. Hence, the ionization of chloride ions in the MB solution contributes to chlorine separation from the MB structure. The remaining MB structure is broken down following oxidation reactions, and common organic intermediates are oxidized into harmless end-products. The suggested photocatalytic mechanism in the MXene-WSe_2 heterostructure involves several key steps, including light absorption, the generation of electrons and holes, charge separation, redox reactions, and the subsequent formation of reaction products, as illustrated in the following sequence,

MXene-WSe2 + hν = electron(-) + hole(+)

WSe_2 + hν = WSe_2(-) + WSe_2(+)

$WSe_2(+) + H_2O = \bullet OH^- + H^+$

Dye + $\bullet OH^-$ = degraded byproducts + CO_2 + H_2O

$WSe_2(-)$ + MXene = WSe_2 + MXene(-)

MXene(-) + O_2 = MXene + $O_2\bullet^-$

Dye + $O_2\bullet^-$ = harmless byproducts + CO_2 + H_2O

4. Summary and conclusions:

In conclusion, we have designed a vertical 2D/2D MXene-WSe_2 heterojunction to evaluate its accessible charge transportation properties through a fabricated junction. AFM, CAFM and STM topography revealed the formation of heterojunctions between two distinct 2D layers. We mapped the vertical heterojunctions by taking STS at different positions within the selected region. The findings provided experimental proof of current rectification via van der Waals vertical heterojunctions between MXene and WSe_2. Also, the internal electrical charge distribution through the M-S junction of the layer was measured by CAFM. This heterostructure system offers efficient charge separation, increased light absorption, and effective reactive species formation by incorporating MXene into WSe_2 and producing a Schottky heterojunction. As a result, the heterostructure exhibited an amplified photocurrent and an enhanced photocatalytic response when exposed to xenon light, resulting in 95.2% degradation of the MB dye within an hour. Our experimental results demonstrate that MXene

can be a cocatalyst in a photocatalytic process based on WSe_2. These results represent a significant step towards making MXenes a viable choice for commercial applications in solar energy utilization.

Data availability statement

The data cannot be made publicly available upon publication because no suitable repository exists for hosting data in this field of study. The data that support the findings of this study are available upon reasonable request from the authors.

Acknowledgement

We thank Prof. Tharangattu N Narayanan and Mr. Dipak Maity, TIFR Hyderabad for the Raman and PL measurements. This work was supported by the SERB, India grant under file no. EEQ/2020/000156. RN acknowledged SERB for funding the project assistant fellowship. AB acknowledges DST India for XRD measurement facilities.

ORCID iDs

Abhijit Bera: https://orcid.org/0000-0003-4898-9797

Rama K Layek: https://orcid.org/0000-0002-9223-049X

References

1. Mas-Ballesté R, Gómez-Navarro C, Gómez-Herrero J and Zamora F (2011) 2D Materials: to Graphene and Beyond. Nanoscale 3:20-30.
2. Gupta A, Sakthivel T and Seal S (2015) Recent Development in 2D Materials Beyond Graphene. Prog. Mater. Sci. 73:44-126.
3. Butler SZ, Hollen SM, Cao L, Cui Y, Gupta JA, Gutierrez HR, Heinz TF, Hong SS, Huang J, Ismach AF, Johnston-Halperin E, Kuno M, Plashnitsa VV, Robinson RD, Ruoff RS, Salahuddin S, Shan J, Shi L, Spencer MG, Terrones M, Windl W and Goldberger JE (2013) Progress, Challenges, and Opportunities in Two-Dimensional Materials Beyond Graphene. ACS Nano 7:2898−2926.
4. Duesberg GS (2014) Heterojunctions in 2D Semiconductors: A Perfect Match. Nat. Mater. 13:1075–1076.
5. Novoselov KS, Mishchenko A, Carvalho A and Castro Neto AH (2016) 2D Materials and Van der Waals Heterostructures. Science 353:6298.

6. Bhunia H, Bera A and Pal AJ (2017) Current Rectification through Vertical Heterojunctions between Two Single-Layer Dichalcogenides (WSe_2|MoS_2 pn-Junctions). ACS Appl. Mater. Interfaces 9: 8248–8254
7. Mak KF, Lee C, Hone J, Shan J and Heinz TF (2010) Atomically Thin MoS_2: A New Direct-Gap Semiconductor. Phys. Rev. Lett. 105:2-5.
8. Pant A, Mutlu Z, Wickramaratne D, Cai H, Lake RK, Ozkan C and Tongay S (2016) Fundamentals of Lateral and Vertical Heterojunctions of Atomically Thin Materials. Nanoscale 8:3870-3887.
9. Guo J, Shi Y, Bai X, Wang X and Ma T (2015) Atomically Thin $MoSe_2$/Graphene and WSe_2/Graphene Nanosheets for the Highly Efficient Oxygen Reduction Reaction. J. Mater. Chem. A 3:24397.
10. Wang K, Huang B, Tian M, Ceballos F, Lin M-W, Mahjouri-Samani M, Boulesbaa A, Puretzky AA, Rouleau CM, Yoon M, Zhao H, Xiao K, Duscher G and Geohegan DB (2016) Interlayer Coupling in Twisted WSe_2/WS_2 Bilayer Heterostructures Revealed by Optical Spectroscopy. ACS Nano 10:6612−6622.
11. Gao A, Liu E, Long M, Zhou W, Wang Y, Xia T, Hu W, Wang B and Miao F (2016) Gate-Tunable Rectification Inversion and Photovoltaic Detection in Graphene/WSe_2 Heterostructures. Appl. Phys. Lett. 108:223501
12. Tang H-L, Chiu M-H, Tseng C-C, Yang S-H, Hou K-J, Wei S-Y, Huang J-K, Lin Y-F, Lien C-H and Li L-J (2017) Multilayer Graphene−WSe_2 Heterostructures for WSe_2 Transistors. ACS Nano 11:12817−12823.
13. Jin J, Xiao T, Zhang Y-F, Zheng H, Wang H, Wang R, Gong Y, He B, Liu X and Zhou K (2021) Hierarchical MXene/Transition Metal Chalcogenide Heterostructures for Electrochemical Energy Storage and Conversion. Nanoscale 13:19740.
14. Hussain S, Vikraman D, Taqi Mehran M, Hussain M, Nazir G, Patil SA, Kim H-S and Jung J (2022) Ultrasonically Derived WSe_2 Nanostructure Embedded MXene Hybrid Composites for Supercapacitors and Hydrogen Evolution Reactions. Renewable Energy 185.
15. Yu X, Pre´vot MS, Guijarro N and Sivula K (2015) Self-Assembled 2D WSe_2 Thin Films for Photoelectrochemical Hydrogen Production. Nat. Commun 6:7596.
16. Chhowalla M, Shin HS, Eda G, Li L-J, Loh KP and Zhang H (2013) The Chemistry of Two-Dimensional Layered Transition Metal Dichalcogenide Nanosheets. Nat. Chem. 5:263−275.

17. Jariwala D, Sangwan VK, Lauhon LJ, Marks TJ and Hersam MC (2014) Emerging Device Applications for Semiconducting Two-Dimensional Transition Metal Dichalcogenides. ACS Nano 8:1102–1120.
18. Li M-Y, Shi Y, Cheng C-C, Lu L-S, Lin Y-C, Tang H-L, Tsai M-L, Chu C-W, Wei K-H, He J-H, Chang W-H, Suenaga K and Li L-J (2015) Epitaxial Growth of a Monolayer WSe_2-MoS_2 Lateral p-n Junction with an Atomically Sharp Interface. Science 349:524-528.
19. Pataniya P, K. Zankat CK, Tannarana M, Sumesh CK, Narayan S, Solanki GK, Patel KD, Pathak VM and Jha PK (2019) Paper-Based Flexible Photodetector Functionalized by WSe_2 Nanodots. ACS Appl. Nano Mater. 2:2758−2766.
20. Li F, Xu B, Yang W, Qi Z, Ma C, Wang Y, Zhang X, Luo Z, Liang D, Li D, Li Z and Pan A (2020) High-Performance Optoelectronic Devices based on van der Waals Vertical MoS_2/$MoSe_2$ Heterostructures. Nano Res. 13:1053–1059.
21. Nag R, Layek RK and Bera A (2022) Functionalized MXene Nanosheets and Al-Doped ZnO Nanoparticles for Flexible Transparent Electrodes. ACS Appl. Nano Mater. 5:17939-17948.
22. Zuo G, Wang Y, Teo WL, Xie A, Guo Y, Dai Y, Zhou W, Jana D, Xian Q, Dong W and Zhao Y (2021) Enhanced Photocatalytic Water Oxidation by Hierarchical 2D-Bi_2MoO_6@2D-MXene Schottky Junction Nanohybrid. Chem. Eng. J. 403:126328.
23. Xiao R, Zhao C, Zou Z, Chen Z, Tian L, Xu H, Tang H, Liu Q, Lin Z and Yang X (2020) In Situ Fabrication of 1D CdS Nanorod/2D Ti_3C_2 MXene Nanosheet Schottky Heterojunction toward Enhanced Photocatalytic Hydrogen Evolution. Appl. catal. B: Environ. 268:118382.
24. Feng X, Yu Z, Sun Y, Shan M, Long R and Li X (2021) 3D MXene/Ag_2S Material as Schottky Junction Catalyst with Stable and Enhanced Photocatalytic Activity and Photocorrosion Resistance Sep. Purif. Technol. 266:118606.
25. Nag R, Bhakuni P and Bera A (2023) Real-Space Observation of an In Situ-Built Schottky Junction in a Two-Dimensional MXene Layer. ACS Appl. Electron. Mater. 5:4759–4769.
26. Nag R, Das D, Manna S, Sasmal S, Thander A and Bera A (2023) Ti_3C_2 MXene Modified Porous $NiTiO_3$ Nanorod Schottky Heterojunction towards Enhanced Photocatalytic Dye Degradation. Mater. Today Commun.:107330.
27. Chen H, Wen Y, Qi Y, Zhao Q, Qu L and Li C (2020) Pristine Titanium Carbide MXene Films with Environmentally Stable Conductivity and Superior Mechanical Strength. Adv. Funct. Mater. 30:1906996.

28. Sun W-J, Zhao Y-Y, Cheng X-F, He J-H and Lu J-M (2020) Surface Functionalization of Single-Layered $Ti_3C_2T_x$ MXene and Its Application in Multilevel Resistive Memory. ACS Appl. Mater. Interfaces 12:9865–9871.
29. Mathis TS, Maleski K, Goad A, Sarycheva A, Anayee M, Foucher AC, Hantanasirisakul K, Shuck CE, Stach EA and Gogotsi Y (2021) Modified MAX Phase Synthesis for Environmentally Stable and Highly Conductive Ti_3C_2 MXene. ACS Nano 15:6420–6429.
30. Hope MA, Forse AC, Griffith KJ, Lukatskaya MR, Ghidiu M, Gogotsi Y and Grey CP (2016) NMR Reveals the Surface Functionalization of Ti_3C_2 MXene. Phys. Chem. Chem. Phys. 18:5099–5102.
31. Sun Y, Jin D, Sun Y, Meng X, Gao Y, Dall'Agnese Y, Chen G and Wang X-F (2018) g-C_3N_4/$Ti_3C_2T_x$ (MXenes) Composite with Oxidized Surface Groups for Efficient Photocatalytic Hydrogen Evolution. J. Mater. Chem. A 6:9124.
32. Ran J, Gao G, Li F-T, Ma T-Y, Du A and Qiao S-Z (2017) Ti_3C_2 MXene Co-Catalyst on Metal Sulfide Photo-Absorbers for Enhanced Visible-Light Photocatalytic Hydrogen Production. Nat. Commun. 8:13907.
33. Xie X, Zhang N, Tang Z-R, Anpo M and Xu Y-J (2018) $Ti_3C_2T_x$ MXene as a Janus Cocatalyst for Concurrent Promoted Photoactivity and Inhibited Photocorrosion. Appl. catal. B: Environ. 237:43-49.
34. Li Y, Ding L, Liang Z, Xue Y, Cui H and Tian J (2020) Synergetic Effect of Defects Rich MoS_2 and Ti_3C_2 MXene as Cocatalysts for Enhanced Photocatalytic H_2 Production Activity of TiO_2. Chem. Eng. J. 383:123178.
35. Cao Y, Fang Y, Lei X, Tan B, Hu X, Liu B and Chen Q (2020) Fabrication of Novel $CuFe_2O_4$/MXene Hierarchical Heterostructures for Enhanced Photocatalytic Degradation of Sulfonamides under Visible Light. J. Hazard. Mater. 387:122021.
36. Nag R, Das S, Das D, Venimadhav A and Bera A (2023) A MXene-$BiFeO_3$-ZnO Nanocomposite Photocatalyst Served as a High-Performance Supercapacitor Electrode. Phys. Chem. Chem. Phys. 25:23125-23132.
37. Chen WY, Jiang X, Lai S-N, Peroulis D and Stanciu L (2020) Nanohybrids of a MXene and Transition Metal Dichalcogenide for Selective Detection of Volatile Organic Compounds. Nat. Commun. 11:1302.
38. Li Q, Yang J, Quhe R, Zhang Q, Xu L, Pan Y, Lei M and Lu J (2018) Ohmic Contacts between Monolayer WSe_2 and Two-Dimensional Titanium Carbides. Carbon 135:125-133.

39. Li Y, Huang S, Wei C, Wu C and Mochalin VN (2019) Adhesion of Two-Dimensional Titanium Carbides (MXenes) and Graphene to Silicon. Nat. Commun. 10:3014.
40. Huang J, Hoang TB and Mikkelsen MH (2016) Probing the Origin of Excitonic States in Monolayer WSe_2. Sci. Rep. 6:22414.
41. Bera A, Dey S and Pal AJ (2014) Band Mapping Across a pn-Junction in a Nanorod by Scanning Tunneling Microscopy. Nano Lett. 14:2000-2005.
42. Feng W, Luo H, Wang Y, Zeng S, Deng L, Zhou X, Zhang H and Peng S (2018) Ti_3C_2 MXene: A Promising Microwave Absorbing Material. RSC Adv. 8:2398-2403.
43. Firestein KL, von Treifeldt JE, Kvashnin DG, Fernando JFS, Zhang C, Kvashnin AG, Podryabinkin EV, Shapeev EV, Siriwardena DP, Sorokin PB and Golberg D (2020) Young's Modulus and Tensile Strength of Ti_3C_2 MXene Nanosheets As Revealed by In Situ TEM Probing, AFM Nanomechanical Mapping, and Theoretical Calculations. Nano Lett. 20:5900–5908.
44. Sierra-Castillo A, Haye E, Acosta S, Bittencourt C and Colomer J-F (2020) Synthesis and Characterization of Highly Crystalline Vertically Aligned WSe_2 Nanosheets. Appl. Sci. 10:874.
45. Li R, Zhang L, Shi L and Wang P (2017) MXene Ti_3C_2: An Effective 2D Light-to-Heat Conversion Material. ACS Nano 11:3752–3759.
46. Yang B, Molina E, Kim J, Barroso D, Lohmann M, Liu Y, Xu Y, Wu R, Bartels L, Watanabe K, Taniguchi T and Shi J (2018) Effect of Distance on Photoluminescence Quenching and Proximity-Induced Spin-Orbit Coupling in Graphene/WSe_2 Heterostructures. Nano Lett. 18:3080-3085.

TOC